Sideband spectroscopy and dispersion measurement in microcavities

Jiang Li, Hansuek Lee, Ki Youl Yang, and Kerry J. Vahala*

T. J. Watson Laboratory of Applied Physics,
California Institute of Technology, Pasadena, California 91125, USA

*vahala@caltech.edu

Abstract: The measurement of dispersion and its control have become important considerations in nonlinear devices based on microcavities. A sideband technique is applied here to accurately measure dispersion in a microcavity resulting from both geometrical and material contributions. Moreover, by combining the method with finite element simulations, we show that mapping of spectral lines to their corresponding transverse mode families is possible. The method is applicable for high-Q, micro-cavities having microwave rate free spectral range and has a relative precision of 5.5×10^{-6} for a 2 mm disk cavity with FSR of 32.9382 GHz and Q of 150 milllion.

OCIS codes: (130.3120) Integrated optics devices; (140.3945) Microcavities; (120.0120) Instrumentation, measurement, and metrology; (300.6380) Spectroscopy, modulation.

References and links

1. K. J. Vahala, "Optical microcavities," Nature **424**, 839–846 (2003).
2. A. B. Matkso, and V. S. Ilchenko, "Optical resonators with whispering-gallery modes-Part I: Basics," IEEE J. Quantum Electron. **12**, 3–14 (2006).
3. V. S. Ilchenko, and A. B. Matkso, "Optical resonators with whispering-gallery modes-Part II: Applications," IEEE J. Quantum Electron. **12**, 15–32 (2006).
4. T. Aoki, B. Dayan, E. Wilcut, W. P. Bowen, A. S. Parkins, T. J. Kippenberg, K. J. Vahala, and H. J. Kimble, "Observation of strong coupling between one atom and a monolithic microresonator," Nature **443**, 671–674 (2006).
5. T. J. Kippenberg, and K. J. Vahala, "Cavity optomechanics: Back-action at the mesoscale," Science **321**, 1172–1176 (2008).
6. F. Vollmer, and S. Arnold, "Whispering-gallery-mode biosensing: label-free detection down to single molecules," Nat. Methods **5**, 591–596 (2008).
7. T. Lu, H. Lee, T. Chen, S. Herchak, J. Kim, S. E. Fraser, R. C. Flagan, and K. Vahala, "High sensitivity nanoparticle detection using optical microcavities," Proc. Natl. Acad. Sci. U.S.A. **108**, 5976–5979 (2011).
8. T. J. Kippenberg, R. Holzwarth, and S. A. Diddams, "Microresonator-based optical frequency combs," Science **322**, 555–559 (2011).
9. W. Liang, V. S. Ilchenko, A. A. Savchenkov, A. B. Matsko, D. Seidel, and L. Maleki, "Whispering-gallery-mode-resonator-based ultranarrow linewidth external-cavity semiconductor laser," Opt. Lett. **35**, 2822–2824 (2010).
10. H. Lee, T. Chen, J. Li, K. Yang, S. Jeon, O. Painter, and K. J. Vahala, "Chemically etched ultrahigh-Q wedge-resonator on a silicon chip," Nat. Photon. **6**, 369–373 (2012).
11. J. Li, H. Lee, T. Chen, and K. J. Vahala, "Characterization of a high coherence, Brillouin microcavity laser on silicon," Opt. Express **20**, 20170–20180, (2012).
12. T. Herr, K. Hartinger, J. Riemensberger, C. Y. Wang, E. Gavartin, R. Holzwarth, M. Gorodetsky, and T. J. Kippenberg, "Universal formation dynamics and noise of Kerr-frequency combs in microresonators," Nat. Photon. **6**, 480–487 (2012).
13. I. Grudinin, A. Matsko, and L. Maleki, "Brillouin lasing with a CaF_2 whispering gallery mode resonator," Phys. Rev. Lett. **102**, 043902 (2009).
14. M. Tomes, and T. Carmon, "Photonic micro-electromechanical systems vibrating at X-band (11-GHz) rates," Phys. Rev. Lett. **102**, 113601 (2009).

#176269 - $15.00 USD Received 17 Sep 2012; revised 31 Oct 2012; accepted 1 Nov 2012; published 7 Nov 2012

15. V. B. Braginsky, M. L. Gorodetsky, and V. S. Ilchenko, "Quality-factor and nonlinear properties of optical whispering-gallery modes," Phys. Lett. A **137**, 393–397 (1989).
16. D. W. Vernooy, V. S. Ilchenko, H. Mabuchi, E. W. Streed, and H. J. Kimble, "High-Q measurements of fused-silica microspheres in the near infrared," Opt. Lett. **23** 247–249 (1998).
17. D. K. Armani , T. J. Kippenberg, S. M. Spillane, and K. J. Vahala, "Ultra-high-Q toroid microcavity on a chip," Nature **421**, 925–928 (2003).
18. A. A. Savchenkov, V. S. Ilchenko, A. B. Matsko, and L. Maleki, "Kilohertz optical resonances in dielectric crystal cavities," Phys. Rev. A **70**, 051804(R) (2004).
19. S. B. Papp, and S. A. Diddams, "Spectral and temporal characterization of a fused-quartz-microresonator optical frequency comb," Phys. Rev. A **84**, 053833 (2011).
20. M. J. Thorpe, R. J. Jones, K. D. Moll, J. Ye, and R. Lalezari, "Precise measurements of optical cavity dispersion and mirror coating properties via femtosecond combs," Opt. Express **13**, 882–888 (2005).
21. A. Schliesser, C. Gohle, T. Udem, and T. W. Hansch, "Complete characterization of a broadband high-finesse cavity using an optical frequency comb," Opt. Express **14**, 5975–5983 (2006).
22. P. Del'Haye, O. Arcizet, M. L. Gorodetsky, R. Holzwarth, and T. J. Kippenberg, "Frequency comb assisted diode laser spectroscopy for measurement of microcavity dispersion," Nat. Photonics **3**, 529–533 (2009).
23. A. A. Savchenkov, E. Rubiola, A. B. Matsko, V. S. Ilchenko, and L. Maleki, "Phase noise of whispering gallery photonic hyper-parametric microwave oscillators," Opt. Express **16**, 4130–4144 (2008).
24. R. G. DeVoe, C. Fabre, K. Jungmann, J. Hoffnagle, and R. G. Brewer, "Precision optical-frequency-difference measurements," Phys. Rev. A **37**, 1802–1805 (1988).
25. J. Li, H. Lee, T. Chen, O. Painter and K. Vahala, "Chip-based Brillouin lasers as spectral purifiers for photonic systems," arXiv:1201.4212 (2011).
26. M. Cai, O. Painter, and K. J. Vahala, "Observation of critical coupling in a fiber taper to silica-microsphere whispering gallery mode system," Phys. Rev. Lett. **85**, 74–77 (2000).
27. S. M. Spillane, T. J. Kippenberg, O. J. Painter, and K. J. Vahala, "Ideality in a Fiber-Taper-Coupled Microresonator system for application to cavity quantum electrodynamics," Phys. Rev. Lett. **91**, 043902 (2003).
28. M. Oxborrow, "Traceable 2-d finite-element simulation of the whispering-gallery modes of axisymmetric electromagnetic resonators," IEEE Trans. Microw. Theory Tech. **55**, 1209–1218 (2007).
29. O. Arcizet, A. Schliesser, P. DelHaye, R. Holzwarth, and T. J. Kippenberg, "Optical frequency comb generation in monolithic microresonators," in *Practical Applications of Microresonators in Optics and Photonics*, ed. A. B. Matsko, (CRC Press, 2009), Ch. 11.
30. G. Agrawal, *Nonlinear Fiber Optics* (Academic Press, 2001).

1. Introduction

Optical microcavities are widely studied across many areas in photonics [1–3] including topics in fundamental science such as cavity QED [4] and cavity optomechanics [5], and in applications such as biosensing [6, 7], microcombs [8] and narrow-linewidth laser sources [9–11]. Beyond Q factor and mode volume, dispersion has become a significant parameter in certain applications. In the subject of microcombs, dispersion determines the spectral maximum of the parametric gain, whether comb oscillation initiates on a native mode spacing, and also microcomb bandwidth at a given pump power [12]. As another example, Brillouin microcavity lasers require careful matching of free spectral range (FSR) with the Brillouin shift [10, 13, 14], and predicting the necessary cavity diameter to achieve this matching requires knowledge of the cavity dispersion. In addition to measurement of cavity dispersion, a wide range of microcavities (including microspheres [15, 16], microtoroids [17], crystalline resonators [18], quartz micromachined resonartors [19], and wedge resonators [10]) feature many transverse mode families, and accurate measurement of FSR can provide a way to map these modes with observable spectral lines.

In microcavities, dispersion has both geometrical (cavity shape) and material contributions, and, as a result, it depends upon the wavelength and the transverse spatial mode family. The measurement of FSR as a function of wavelength provides a convenient way to characterize cavity dispersion. Along these lines, frequency combs have provided a powerful way to measure dispersion in cavities that can be approximately matched in FSR to the comb repetition frequency [20, 21]. Also, in cases where this is not possible, a frequency-comb has been used together with a tunable-diode-laser to measure FSR and dispersion [22]. These techniques,

#176269 - $15.00 USD Received 17 Sep 2012; revised 31 Oct 2012; accepted 1 Nov 2012; published 7 Nov 2012

while providing fast, accurate and wide band dispersion measurement, require access to a stabilized frequency comb. In another method, "white light", filtered to a 1 nm bandwidth, has been used for dispersion measurement in a CaF_2 whispering gallery microcavity [23]. Multiple RF beat notes are produced that contain the contribution of all the WGM modes (with different transverse order and azimuthal order) in the 1 nm bandwidth probed. This is a convenient way to measure dispersion, but the method does not enable correspondence of the optical spectral peaks with the RF beat notes. In this letter, we modify a method that has been used to measure FSR and mirror-induced dispersion in a Fabry-Perot [24] to the case of a microresonator. In that method two FM sidebands were imposed on an optical carrier and then separately tuned so as to attain locking with two cavity modes. In the present work we use a single modulation in combination with a reference interferometer. While not attaining the same level of precision in the earlier work, the present technique does not require locking to the resonator modes and provides sufficient precision to measure both the spectral and transverse mode dependence of dispersion in a high-Q silica microresonator. The technique can be applied in resonators with FSR in the microwave rate range.

2. Measurement method and uncertainty analysis

A lithium niobate phase modulator and a microwave source are used to generate a sinusoidally, phase modulated signal on a probe laser at a modulation rate f_m close to the FSR of the resonator such that $FSR > f_m$ (see Fig. 1(a)). The probe laser is an external cavity diode laser and is scanned across a cavity resonance so as to produce the oscilloscope trace of the transmitted power shown in Fig. 1(b). When the phase modulation is "off", the transmission spectrum of the cavity has the single Lorentzian line shape as shown in Fig. 1(b) (red curve). However, when the phase modulation is "on", the transmission spectrum will show three spectral peaks as the two side peaks come from the phase modulation sidebands that are coupled to the cavity through the neighboring resonances of the initial cavity resonance. The offset frequency ($\Delta f = FSR - f_m$) is then measured by using a Mach-Zehnder interferometer (MZI) to create a fringe-like reference spectrum. If T_d and T_m are corresponding oscilloscope time intervals for the offset frequency and neighboring MZI fringe maxima, then the offset frequency is given by $\Delta f = \frac{T_d}{Tm} FSR_M$, where FSR_M is the FSR of the MZI. Upon determination of the offset frequency, the cavity FSR is determined by $FSR = f_m + \Delta f$.

Using the above results, the uncertainty of cavity FSR is given by,

$$\delta FSR = \delta f_m + \frac{T_d}{Tm}\delta FSR_M + \frac{\delta T_d}{Tm} FSR_M + \frac{T_d \delta T_m}{T_m^2} FSR_M \tag{1}$$

The first term on the R.H.S of Eq. (1) is the uncertainty of the modulation frequency. It is determined by frequency uncertainty of the RF synthesizer, which is negligible compared with the other terms (less than 1Hz).

Concerning the second term in Eq. (1), the FSR of the MZI is measured to kHz level uncertainty by sending a CW external-cavity diode laser into the MZI and measuring the power spectral density (PSD) using a balanced photodetector. When the laser frequency is set to the quadrature point of the MZI, the frequency noise of the laser is discriminated by the MZI fringes. As shown in [10, 25] the PSD is then proportional to $sinc^2(\tau_d f)$, where $\tau_d = \frac{1}{FSR_M}$ is the delay on the MZI. Thus the periodic spectral minima of the PSD can be used to extract the MZI FSR accurately. Fig. 2(a) gives the spectrum of the MZI outputs from 110 MHz - 200 MHz, which spans the 17th to 29th spectral minima of the MZI. The frequency location of each minima was divided by its order to create the plot of MZI FSR values in Fig. 2(b). The average MZI FSR is 6.723 MHz $\pm$ 2.7kHz. The offset frequency, Δf , is about 1 - 5 times the FSR of the MZI, which means $\frac{T_d}{Tm} \approx$ 1 - 5. As a result, the error contribution from the second term in

#176269 - $15.00 USD Received 17 Sep 2012; revised 31 Oct 2012; accepted 1 Nov 2012; published 7 Nov 2012

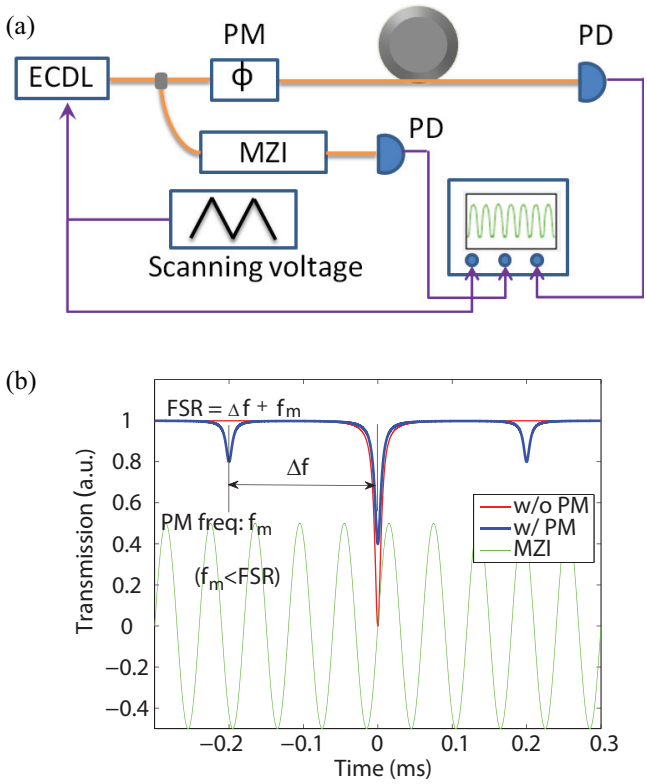

Fig. 1. **Experimental setup.** (a) A schematic is shown for the sideband spectroscopy method used to measure dispersion. A phase modulator (PM) creates sidebands on a probe laser that are set to coincide approximately with the cavity FSR. Also, a Mach-Zehnder interferometer creates a reference spectrum to measure the offset frequency Δf. The laser is scanned so as to produce the spectrum shown in panel (b). (b) Schematic traces of the sideband spectroscopy are shown. When the phase modulation is "off" the red trace is observed showing that the laser is scanning through a single cavity resonance. With the phase modulation "on" and with its frequency set to be close in value to the cavity FSR, three spectral peaks appear as the two phase modulation sidebands scan through their respective cavity resonances (neighboring the resonance probed by the scan-laser, carrier wave). By using the green interferometer trace to measure the offset Δf and adding this offset to the phase modulation frequency, the cavity FSR can be measured.

Eq. (1) is no larger than ± 15 kHz.

Finally, we consider the error contributions from the third and fourth terms in Eq. (1). In practice, these errors are on the order of 100 kHz in our measurement, based on repetitive measurements of the cavity FSR for one specific cavity mode using the method described above. For instance, 10 measurement of a 6 mm disk resontor with a cavity Q of 200 million gives an FSR of 10.8230 GHz ± 109kHz. As a result, the overall uncertainty in measurement of microcavity FSR is set by these contributions.

#176269 - $15.00 USD Received 17 Sep 2012; revised 31 Oct 2012; accepted 1 Nov 2012; published 7 Nov 2012

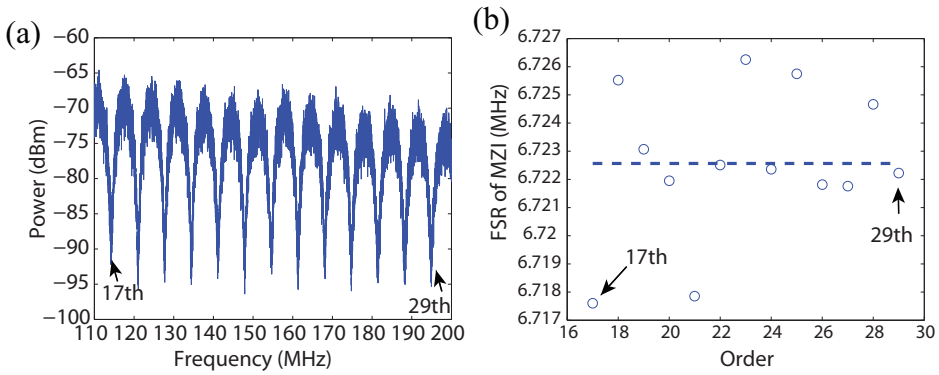

Fig. 2. **Measurement of the FSR of the Mach Zehnder interferometer (MZI).** (a) Measured power spectrum of the photocurrent output from a balanced photodetector whose inputs detect the complementary outputs of the MZI. For this measurement the laser frequency is close to a quadrature point of the MZI and the spectral measurement extends from 110-200 MHz. (b) FSR of the MZI extracted from each order in (a). The dashed line is the average.

3. Cavity transverse mode spectroscopy

We apply the above approach to measure the FSR of different transverse modes of the same cavity. Comparison to finite element modeling then enables a mapping of spectral peaks with spatial modes of the resonator. The TE modes of a 6 mm wedge resonator (FSR of approximately 10.8 GHz) are characterized. Details on the fabrication and properties of this resonator are presented in [10]. Briefly, however, these silica-based devices are fabricated on a silicon wafer using only lithography and a combination of wet and dry etching. They have optical Q factors ranging from several hundred million to nearly 1 billion. Their cross section is wedge-like and the device characterized in Fig. 3 has a wedge angle $\alpha \approx 12^{\circ}$ in a silica oxide with thickness $T \approx 10$ μm (measured using an SEM). Schematic cross sections of the device showing three transverse modes are illustrated in Fig. 3(d). Optical coupling uses a fiber taper coupler [26,27].

In Fig. 3(a) a spectral scan encompassing one FSR is shown. By scanning over two FSRs it is possible to identify repeating peaks that are associated with a particular transverse mode family. The various spectral peaks shown correspond to distinct transverse modes of the device, and are labeled from A to J. In Fig. 3(b) a "zoom-in" spectrum in the vicinity of peak G is shown to illustrate the measurement technique detailed in Fig. 1. Also shown in Fig. 3(b) is the Mach-Zehnder reference trace. Measurement results giving the FSR for each transverse mode are provided in Fig. 3(c) (data are circles). Note that the transverse mode dispersion introduces a difference of about 1 MHz in the FSR of neighboring transverse modes. This difference is easily resolved as the measurement uncertainty is about 100 kHz (see discussion in previous section). In order to identify the cavity modes, we calculate the FSR of different transverse-order modes by FEM simulation in a commercial FEM solver (COMSOL multiphysics). The simulation method is based on the 2D simulation of the whispering-gallery modes (WGM) of axisymmetric resonators described in [28]. The calculated FSR values are plotted in Fig. 3(c) for three, slightly-different, cavity dimensions (wedge angle and disk thickness). Several other geometries were also simulated, however, the three shown gave the best agreement over the range of modes measured. From the three FEM plots (indicated by triangles, diamonds, and squares), it can be seen that a small perturbation of the cavity dimension maintains the FSR sequence of different orders. Moreover, the three FEM plots are in reasonable agreement with

#176269 - $15.00 USD Received 17 Sep 2012; revised 31 Oct 2012; accepted 1 Nov 2012; published 7 Nov 2012

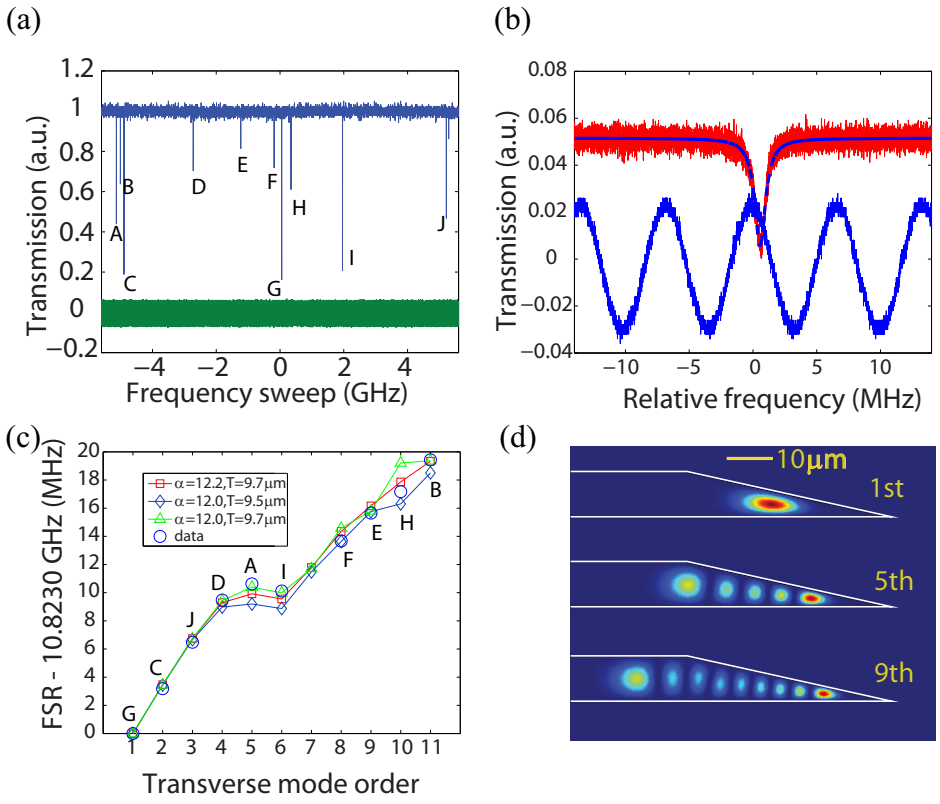

Fig. 3. **Cavity transverse mode spectroscopy** (a) Transmission spectrum for a 6 mm wedge resonator. Multiple transverse modes (labeled from A to J) are shown within the frequency sweep of one FSR (10.8 GHz). The lower green trace is the Mach-Zehnder reference inteferometer (MZI) (FSR of the MZI is 6.723 MHz, MZI fringes are resolved in panel (b)). By using the MZI fringes and the calibrated MZI FSR, the original horizontal axis (time span, as shown in Fig. 1(b)) can be converted to frequency span. (b) Zoom-in measurement of the peak G in panel (a). The Lorentzian fit shows a loaded cavity linewidth of 1.03 MHz. This is also the fundamental mode indicated in panels (c) and (d). (c) Mapping of the cavity transverse-order to each spectral peak by comparing the FSR measurement with FEM simulation. Three slightly different cavity geometries are used for FEM simulation, and the FSR of the simulated transverse modes maintains the sequence regardless of geometry. (d) Intensity profile of the 1st, 5th and 9th transverse-order modes calculated by FEM. The corresponding spectral peaks are given to the right of the profile.

the data. (The 7th transverse mode order is not identified. The reason may be due to unfavorable coupling position or phase match of taper-fiber coupling). Through this comparison it was possible to map each spectral peak to a particular transverse mode family. Several identifications have been made in Fig. 3(d), including the fundamental mode "G". It is interesting to note that this fundamental mode has the smallest FSR of all of the modes. This is expected since the fundamental mode should also exhibit the largest effective index. Also, the slight plateau in the FSR versus mode order (see Fig. 3(c)) is associated with the higher-order-modes extending radially inward beyond the wedge region.

This mapping is based on the increment of the FSR of each transverse mode order; and if the

#176269 - $15.00 USD Received 17 Sep 2012; revised 31 Oct 2012; accepted 1 Nov 2012; published 7 Nov 2012

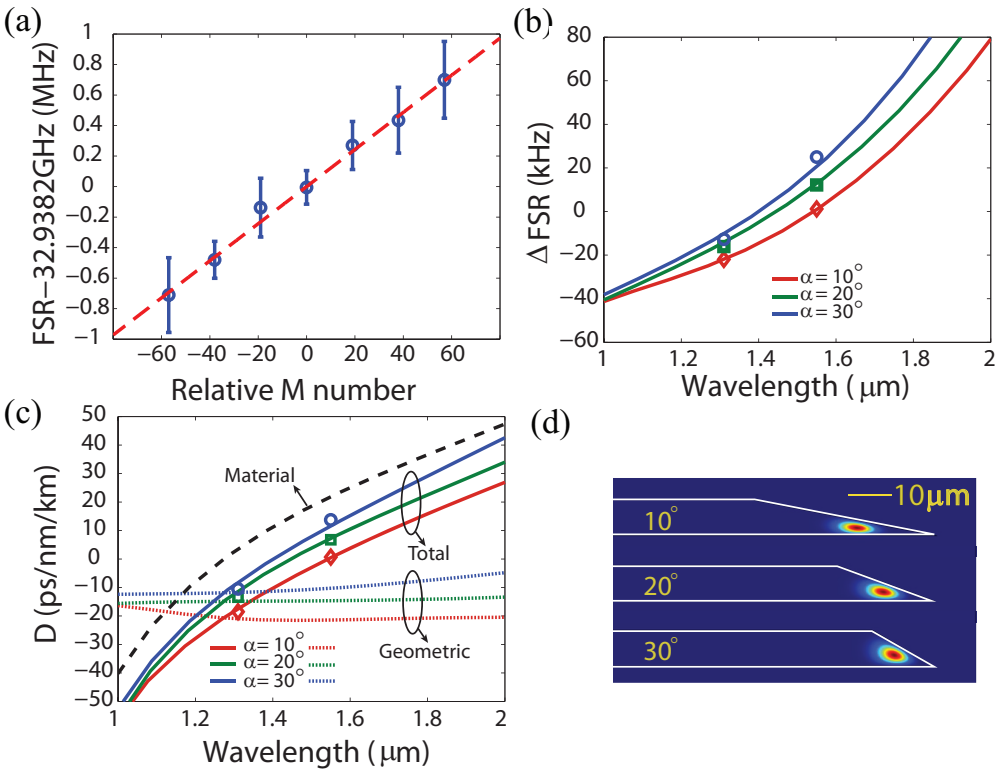

Fig. 4. **Measurement of dispersion at two wavelengths for three cavity geometries.** (a) Measured cavity FSR (wrt 32.9382 GHz) for 2 mm resonator ($\alpha \approx 20°$, oxide thickness, T $\approx 8\mu$m) plotted versus relative azimuthal mode number M around the 1550 nm spectral region. The dashed, red line is a linear fit giving 12.2 kHz/FSR dispersion. (b) Measured (colored makers) and simulated cavity dispersion, ΔFSR, as a function of wavelength for 2 mm disk resonators with three wedge angles ($\alpha \approx 10°$, $20°$ and $30°$, T $\approx 8\mu$m). (c) Solid lines give the dispersion parameter, D, converted from the ΔFSR values in (b), using $\Delta FSR \approx \frac{c^2\lambda^2 D}{4\pi^2 n^3 R^2}$ [29]. The dashed line is the silica material dispersion from the Sellmeier equation. The three dotted lines are the geometric dispersion, obtained by subtracting the material dispersion from the total dispersion. The measurement data points are given as markers. (d) Intensity profile for 2 mm resonators with $10°$, $20°$ and $30\ °$ wedge angles.

FSRs between two neighboring pairs of transverse modes are close to each other, for example, the 4-6th modes in Fig. 3(c), the modes may not be mapped accurately. The labeling of spectral peaks "D, A, I" to mode order 4, 5, and 6 is therefore only one possible mapping. However, having the FSR of each transverse mode is important by itself and can differentiate between low order and high order modes. It can be particularly usefully in studying stimulated Brillouin lasers [11] and microcomb generation in microresonators [8, 22].

4. Dispersion characterization of wedge disk resonators

To measure the dispersion within a single transverse mode family, the above technique is repeated for a sequence of spectral peaks having the same transverse mode order. However, because the FSR dispersion of these resonators, $\Delta FSR = FSR_m - FSR_{m-1}$, is usually very small (in the order of 1-10 kHz/FSR, depending on the resonator diameter), it is necessary to mea-

#176269 - $15.00 USD Received 17 Sep 2012; revised 31 Oct 2012; accepted 1 Nov 2012; published 7 Nov 2012

sure the cavity FSR over multiple FSR separations. Fig. 4(a) shows the cavity FSR for a 2 mm cavity ($\alpha \approx 20^\circ$, T $\approx 8\ \mu$m) plotted versus the relative cavity azimuthal mode number M (FSR number) measured around the 1550 nm region. The dashed line is a linear fit which gives a dispersion of 12.2 kHz/FSR. This value is in good agreement with the simulated value (12.8 kHz/FSR, simulation is based on the 2D FEM solver of the whispering-gallery modes of axisymetric microcavities as described in [28]). The RMS error of the FSR measurement is 180 kHz (for a cavity Q of 150 million), which gives a relative precision of 5.5×10^{-6} for a cavity FSR of 32.9382 GHz. In Fig. 4(b) measurements of the FSR dispersion of disk resonators with three different wedge angles ($\alpha \approx 10^\circ, 20^\circ, 30^\circ$) and at two different wavelengths (1550nm and 1310nm) are presented along with the calculated ΔFSR. Fig. 4(c) converts the FSR dispersion values to the more widely used dispersion parameter, $D \equiv \frac{d}{d\lambda}\left(\frac{1}{v_g}\right)$, using $\Delta FSR \approx \frac{c^2\lambda^2 D}{4\pi^2 n^3 R^2}$ [29], where R is the cavity radius, n is the refractive index and λ is the wavelength. Also, the material dispersion parameter, D_M (calculated from the Sellmeier equation [30]), and the geometric dispersion parameter ($D_G = D - D_M$) are plotted. From Fig. 4(b) and (c), it can be seen that the measurement data (in markers) agree reasonably well with the simulation. Also, note that resonators having smaller wedge angles feature larger geometrical dispersion. This is consistent with the centroid of the mode's "orbit" around the resonator being shifted radially inward as wavelength increases, and hence smaller wedge angles enhancing this tendency.

5. Conclusion

In conclusion, we have demonstrated a simple and accurate approach to measure the FSR of microcavities by introducing external phase modulation and frequency calibration with an MZI. This FSR measurement method is applicable for high-Q resonators with microwave rate FSR and has a precision of 5.5×10^{-6} (given a cavity Q of 150 million). We have used this approach to measure the FSRs of different cavity transverse modes and find that the cavity transverse mode can be identified from their FSRs when comparing with FEM simulation results. Finally, we have applied the FSR-measurement approach to characterize cavity dispersion, which is important in many nonlinear photonic applications, such as the generation of microcombs.

Acknowledgments

The authors acknowledge the financial support from the DARPA QuASAR program, the Institute for Quantum Information and Matter, an NSF Physics Frontiers Center with support of the Gordon and Betty Moore Foundation, NASA and the Kavli NanoScience Institute.

#176269 - $15.00 USD Received 17 Sep 2012; revised 31 Oct 2012; accepted 1 Nov 2012; published 7 Nov 2012